Electronic Spectra, Excited-State Geometries, and Molecular Electrostatic Potentials of Hypoxanthine: A Theoretical Investigation†

M. K. Shukla and Jerzy Leszczynski*

Computational Center for Molecular Structure and Interactions, Department of Chemistry, Jackson State University, Jackson, Mississippi 39217

Received: July 31, 2002; In Final Form: May 7, 2003

The ground-state geometry of hypoxanthine was optimized at the MP2, B3LYP, and HF levels by employing the 6-311++G(d,p) basis set. The vertical singlet transition energies were calculated at the CASSCF/6-31+G(d), TD-B3LYP/6-311++G(d,p), and CIS/6-311++G(d,p) levels by using the MP2-, B3LYP-, and Hartree−Fock-optimized geometries, respectively. In the case of the CASSCF calculations, the active space consisted of the 2σ, 6π, and $4\pi^*$ orbitals. The σ orbitals were used to compute the nπ^* transitions. The effects of dynamic correlation on the CASSCF energies were considered at the second-order multiconfigurational quasi-degenerate perturbation (MCQDPT2) theory. The effect of hydration was considered by including three water molecules in the first solvation shell of hypoxanthine. The geometry of the molecule was also optimized in the lowest singlet $\pi\pi^*$ and nπ^* excited states at the CIS/6-311++G(d,p) level. The characteristics of the ground and excited-state potential energy surfaces were ascertained from a harmonic vibrational analysis in the respective states. The molecular electrostatic potentials were computed in the ground and vertical singlet $\pi\pi^*$ and nπ^* excited states. The computed vertical singlet transition energies are found to be in good agreement with the corresponding experimental data. It has been suggested that hypoxanthine has a weak $\pi\pi^*$ transition near 225 nm. The geometry of the molecule is found to be highly nonplanar in the lowest singlet $\pi\pi^*$ excited state and approximately planar in the lowest singlet nπ^* state, except for the CO group which is displaced appreciably out-of-plane from the ring plane. Hydration does not have a significant effect on the geometry of the isolated molecule. The molecular electrostatic potentials are found to be altered in going from the ground to different vertical singlet excited states. Significant reduction in the electrostatic potential magnitude near the carbonyl oxygen site of the molecule is found in the lowest singlet nπ^* excited state.

1. Introduction

Professor Michel Kasha is a pioneer in the electronic spectroscopy of complex molecular systems.[1] He has charted a path in photophysical research that many have followed. The famous "Kasha's rule" states that "the emitting level of a given multiplicity is the lowest excited level of that multiplicity."[2] He first demonstrated the biprotonic transfer reaction in the 7-azaindole dimer under electronic excitation in 1969.[3] The present work, a theoretical study of the excited-state properties of hypoxanthine, is dedicated to Professor Kasha as a tribute to his continuous stimulating influence in the area of photophysics of complex biomolecular systems.

This article is a continuation of our efforts in the studies of the excited states of purines and pyrimidines through geometry optimization.[4] Such studies are important because the knowledge of excited-state geometries by experimental determination is not possible for molecules of these sizes. Experimental studies, for example, have indicated a nonplanar excited-state geometry for the pyrimidines,[5] and such predictions have been supported by theoretical studies.[6] It is well-known that ultraviolet (UV) radiation is very harmful for living systems and the level of UV radiation is increasing as the layer of ozone is depleted.[7] One of the most common and frequently UV-induced damage to DNA is the formation of pyrimidine dimers.[8] Another effect of UV irradiation may be the formation of rare tautomers of nucleic acid bases through photoexcitation, which are believed to play an important role in point mutations.[9]

Hypoxanthine is a purine metabolic intermediate in living systems.[10] Its nucleotide analogue, inosinate, is the precursor of adenylate and guanylate.[10] In DNA, it is highly mutagenic; during DNA replication it can code for guanine and forms a base pair with cytosine.[11] Structurally, hypoxanthine is closer to guanine and can be formed by the deamination of guanine.[10] It is also found as a minor purine base in transfer RNA.[12] Hypoxanthine and guanine both exhibit keto−enol and N9H−N7H tautomerism.[13] However, the concentration of the enol tautomer is much higher in the case of guanine compared to the concentration of the same tautomer in hypoxanthine.[13b] Different quantum chemical computations in the gas phase,[14] matrix isolation studies,[13] photoelectron spectra,[15] and NMR studies in dimethyl sulfoxide[16] have suggested that the keto-N7H form of hypoxanthine is more prevalent than the keto-N9H form (a hydrogen is attached at the N1 site for both forms). The existence of a small amount of the enol-N9H form of hypoxanthine has also been suggested by using both theoretical and experimental techniques.[13,14] Theoretical calculations suggest that under aqueous solvation, the keto-N9H form is favored over the keto-N7H form and the enol-N9H form is largely destabilized.[14] The UV-spectroscopic study in water also predicts the domination of the keto-N9H form over the keto-N7H form.[17] In a crystalline environment, hypoxanthine exists as the keto-

† Manuscript submitted in honor of Professor Michel Kasha.

* Corresponding author. E-mail: jerzy@ccmsi.us.

10.1021/jp021781o CCC: $25.00
Published on Web 07/01/2003

N9H tautomeric form.[18] Earlier we have performed a detailed theoretical study of four hypoxanthine tautomers (keto-N1HN9H, keto-N1HN7H, enol-N1HN9H, and enol-N1HN7H) at the Hartree−Fock (HF), DFT-B3LYP, and MP2 levels employing the 6-31G(d,p) and 6-311++G(d,p) basis sets to estimate the relative stability, concentration, tautomerization constant, and the barrier height for proton transfers and the effect of hydration on them.[14a,b] The barrier height of tautomerization was found to be reduced significantly with the inclusion of a water molecule in the proton-transfer reaction path.[14a,b] We have also shown that the transition state corresponding to a proton transfer from the keto form to the enol form of the hydrated species has a zwitterionic structure. These results were found to be in accordance with the molecular dynamics simulation study of proton transfer in a protonated water chain, which was described in the form of the collective movement of protons in terms of either the H_3O^+ type or the $H_5O_4^+$ type.[19] Experimental studies of proton transfer on the 7-azaindole dimer have also suggested the zwitterionic type of transition-state structure.[20]

It is generally known that the 260 and 200 nm absorption bands of purines consist of two transitions with nonparallel transition dipole moments; the relative intensity and positions are dependent on the environment.[21,22] Occasionally, a weak transition near 225 nm is also observed, which is considered to be the weak $\pi\pi^*$ or the $n\pi^*$ type.[21,23] In this paper, we have performed investigations of the excited-state properties and excited-state geometries of the natural form of hypoxanthine (keto-N9H form) at the CASSCF level including the second-order multiconfigurational quasi-degenerate perturbation theory (MCQDPT2) level of dynamic correlation to energy, at the TD-B3LYP level, and at the CIS level with the aim of studying the following: (i) the performance of different methods in the interpretation of electronic transitions, (ii) the geometry of molecules in the lowest singlet $\pi\pi^*$ or $n\pi^*$ electronic excited states, (iii) the interaction of water molecules in the excited state, and (iv) molecular electrostatic potential (MEP) maps in the ground and different excited states. We have considered three water molecules in the first solvation shell of the hypoxanthine.

2. Computational Details

The ground-state geometries of hypoxanthine were optimized at the HF, B3LYP, and MP2 levels of theories by employing the 6-311++G(d,p) basis set and were found to have planar (C_s) symmetry. The geometry of the hydrated form of the molecule considering three water molecules in the first solvation shell was also optimized at the HF/6-311++G(d,p) and B3LYP/6-311++G(d,p) levels. The CASSCF level of theory employing the 6-31+G(d) basis set and planar (C_s) symmetry was used to compute vertical singlet transition energies of the molecule. The ground-state optimized geometry at the MP2/6-311++G(d,p) level was used for the CASSCF calculations. The CASSCF active space consisted of the 2σ, 6π, and $4\pi^*$ orbitals. The σ orbitals were used to compute the $n\pi^*$ transitions. The CASSCF energies were obtained by giving 100% weight to each state except for the third and fifth singlet $\pi\pi^*$ excited states, for which the weight factors were 88 and 96.5%, respectively. Several attempts were made to compute these states with 100% weight, but convergence was not obtained. The effects of dynamic correlation on the CASSCF energies were considered using the MCQDPT2 theory.[24]

The vertical singlet transition energies were also computed at the CIS[25] and TD-B3LYP[26] levels by using the HF- and B3LYP-optimized geometries, respectively. The geometries of the lowest singlet $\pi\pi^*$ excited state of the isolated and hydrated forms were optimized at the CIS level. The nature of the stationary points was ascertained by harmonic vibrational frequency analysis both in the ground and excited states. The Gaussian cubegen utility was used to generate electrostatic potential and electron density cube files in the ground and excited states. The electron density difference cubes were generated using the Gaussian cubman utility by subtracting the ground-state density cube obtained at the HF/6-311++G(d,p) level from the vertical singlet excited-state density cube obtained at the CIS/6-311++G(d,p)//HF/6-311++G(d,p) level. The MEP and electronic density mappings and the analysis of MEP values were performed using the gOpenMol program.[27] The 6-311++G(d,p) basis set and Gaussian 94 and Gaussian 98 suites of programs were used for all but the CASSCF calculations.[28] The CASSCF calculations were performed using the GAMESS package.[29] It is well-known that linear scaling is needed for the CIS transition energies to compare the energies with the corresponding experimental data.[4a,b,30] A factor of 0.72 has been found satisfactory for purines and pyrimidines, and we have used the same scaling factor in this case also.[4a,b,30]

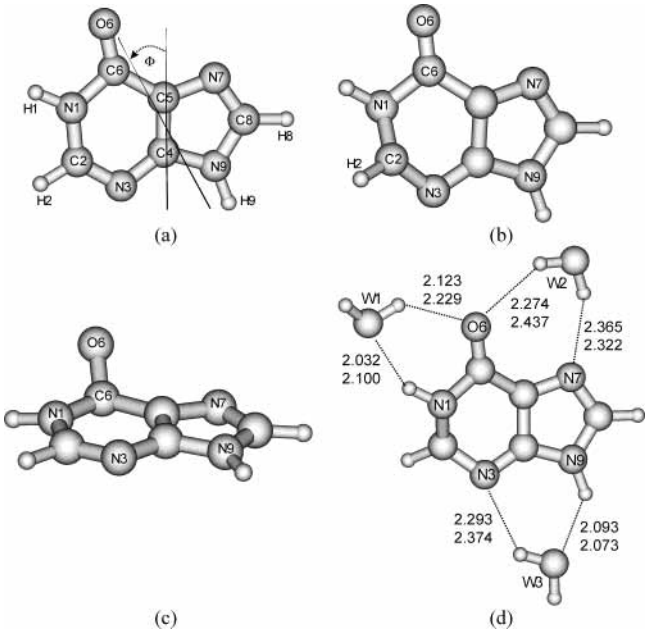

Figure 1. (a) Structure and atomic numbering schemes of hypoxanthine; the Φ shows the transition moment direction according to Tinoco−DeVoe convention, (b) geometry in the lowest singlet $\pi\pi^*$ excited state, (c) geometry in the lowest singlet $n\pi^*$ excited state, and (d) geometry of hydrated form in the lowest singlet $\pi\pi^*$ excited state. The upper indices represent ground state and the lower indices represent excited-state parameters.

3. Results and Discussion

The structure and atomic numbering schemes of hypoxanthine are shown in Figure 1. The ground-state geometry of hypoxanthine was found to be planar at all applied levels, namely the MP2/6-311++G(d,p), B3LYP/6-311++G(d,p), and HF/6-311++G(d,p) approximations. The computed ground-state dipole moment was found to be 4.72, 5.13, 5.07, and 5.22 D at the CASSCF/6-31+G(d)//MP2/6-311++G(d,p), MP2/6-311++G(d,p), B3LYP/6-311++G(d,p), and HF/6-311++G(d,p) levels, respectively. The experimental measurement of the dipole moment of hypoxanthine was performed in acetic acid, and the measured value is 3.16 D.[31] Therefore, the CASSCF-computed dipole moment is relatively closer to the experimental value than those obtained from the other methods.

TABLE 1: Computed and Experimental Transition Energies (ΔE; eV), Dipole Moments (μ; Debye), Oscillator Strengths (f), and Transition Moment Directions (Φ;°), According to Tinoco−DeVoe Convention of Hypoxanthine

MCQDPT2	CASSCF		CIS[a]									TD-B3LYP								
isolated	isolated		isolated					hydrated				isolated			hydrated			experimental[b]		
ΔE	ΔE	μ	ΔE	ΔE^1	f	Φ	μ	ΔE	ΔE^1	f	Φ	ΔE	f	Φ	ΔE	f	Φ	ΔE^2	ΔE^3	ΔE^4
$\pi\pi^*$ transitions																				
4.63	5.62	2.66	6.11	4.40	0.247	−61	4.31	6.20	4.46	0.209	−57	4.75	0.139	−74	4.82	0.100	−78	4.41	4.46	4.59−4.77
5.35	6.55	4.66	6.95	5.00	0.362	56	6.68	6.89	4.96	0.427	54	5.43	0.146	43	5.36	0.141	41	5.19	5.02	4.98
5.48	6.92	3.80	7.35	5.29	0.045	24	4.61	7.49	5.39	0.016	8	6.22	0.003	−66	6.29	0.038	−3	5.51[c]		
5.78	7.97	5.87	8.07	5.81	0.102	20	4.31	8.12	5.85	0.100	26	6.44	0.065	34	6.34	0.023	24	6.05	6.26	6.20
6.31	8.40	6.83	8.43	6.07	0.034	77	4.32	8.53	6.14	0.175	68	6.89[d]	0.116	47	6.74	0.410	64	6.42	6.70	
$n\pi^*$ transitions																				
5.75	6.62	3.45	6.88	4.95	0.0001		3.12	7.19	5.18	0.0001		5.26	0.0001		5.41	0.0015				
6.06	7.19	4.84	7.50	5.40	0.0036		6.90	7.72	5.56	0.0042		5.30	0.0001		5.47	0.0007				

[a] ΔE^1 represents scaled transition energies (scaling factor 0.72). [b] Absorption transition of 9-methylhypoxanthine, ΔE^2 = vapor phase, ΔE^3 = in trimethyl phosphate solution, ΔE^4 = in water at pH 6.1 [ref 33a]. [c] From the CD measurement of deoxyinosine 5′-phosphate [ref 23]. [d] Rydberg contamination.

TABLE 2: CASSCF Natural Orbital Occupation Numbers for Hypoxanthine in the Ground and Excited States

state[a]	1n	2n	3π	4π	5π	6π	7π	8π	9π	10π	11π	12π
S_0	1.998	1.998	1.994	1.988	1.949	1.940	1.957	1.911	0.041	0.075	0.082	0.067
1-$\pi\pi^*$	1.987	1.998	1.976	1.999	1.947	1.886	1.941	1.378	0.048	0.620	0.140	0.079
2-$\pi\pi^*$	1.999	1.998	1.988	1.985	1.938	1.925	1.657	1.170	0.805	0.383	0.099	0.054
3-$\pi\pi^*$	1.999	1.998	1.990	1.979	1.914	1.847	1.624	1.279	0.662	0.439	0.198	0.072
4-$\pi\pi^*$	1.999	1.998	1.981	1.962	1.948	1.911	1.631	1.202	0.766	0.368	0.171	0.063
5-$\pi\pi^*$	1.999	1.998	1.976	1.954	1.937	1.881	1.638	1.317	0.743	0.378	0.114	0.064
1-nπ^*	1.048	1.951	1.992	1.994	1.971	1.944	1.874	1.951	0.978	0.166	0.087	0.044
2-nπ^*	1.693	1.306	1.993	1.993	1.962	1.950	1.938	1.887	0.755	0.399	0.080	0.043

[a] Numbers 1,2,3... represent corresponding singlet excited state in ascending order of energy.

The experimental dipole moments of purines and pyrimidines are found to be solvent dependent.[31] Therefore, the calculated discrepancy in our case might be due to the nature of the observed dipole moment of purines,[31] which is dependent on the solvent or may be due to the presence of minor tautomers of the molecule in acetic acid.[13−17]

3.1. Electronic Transitions. The vertical singlet $\pi\pi^*$ and nπ^* transition energies of hypoxanthine obtained at different levels of theories are presented in Table 1 along with selected experimental data. Some transitions of the $\pi\sigma^*$/Rydberg type[32] were also obtained at the CIS and TD-B3LYP levels but are not presented here. The CASSCF natural orbital occupation numbers for the ground and singlet excited states are shown in Table 2. In this table, 1n and 2n represent lone pair orbitals, $3\pi-8\pi$ are occupied π orbitals, and $9\pi-12\pi$ are virtual π^* orbitals. Table 2 suggests that, generally, the HOMO−1, HOMO, LUMO, and LUMO+1 orbitals ($7\pi-10\pi$) are involved in the singlet $\pi\pi^*$ excitation processes. Contributions from the HOMO and LUMO orbitals are largest and play a major role in the excitation processes. In some cases, small contributions from the HOMO−2 and LUMO+2 orbitals (6π and 11π) are also revealed (Table 2).

A comparison of the singlet $\pi\pi^*$ transition energies obtained using different methods suggests that there is good correspondence between the MCQDPT2 and scaled CIS transition energies within an accuracy of about 0.2 eV, except for the second transition for which the margin of error is larger (Table 1). Although the first two $\pi\pi^*$ transition energies obtained through the TD-B3LYP method are in good agreement with the corresponding MCQDPT2 and scaled CIS data, the higher transitions show significant error (Table 1). Experimental absorption transitions of 9-methylhypoxanthine obtained in the vapor phase, in trimethyl phosphate, and in water are presented in Table 1 for comparison.[33] The computed MCQDPT2 transition energies at 4.63, 5.35, 5.78, and 6.31 eV are in good agreement (within an accuracy of 0.2 eV) with the experimental transition energies of 9-methylhypoxanthine in the vapor phase near 4.41, 5.19, 6.05, and 6.42 eV (Table 1). The computed transition energies of hypoxanthine at the TD-B3LYP level at 4.75, 5.43, 6.44, and 6.89 eV and at the CIS level at 4.40, 5.00, 5.81, and 6.07 eV (scaled values) can also be correlated satisfactorily with the vapor phase experimental data (Table 1). However, the margin of error is larger than for those obtained at the MCQDPT2 level. The absorption of 9-methylhypoxanthine in an aqueous solution with a pH of 6.1 shows a broad shoulder in the range of 4.59−4.77 eV and peaks near 4.98 and 6.20 eV.[33a] The computed transition energies of hydrated hypoxanthine at the TD-B3LYP level at 4.82, 5.36, and 6.34 eV and at the CIS level at 4.46, 4.96, and 5.85 eV (scaled values) can be compared with the corresponding experimental data of 9-methylhypoxanthine in aqueous solution (Table 1). The TD-B3LYP results are in good agreement with the experimental data except for the second transition for which the margin of error is larger. On the other hand, the CIS results agree better for the lower transitions. The computations also predict the existence of a weak $\pi\pi^*$ transition in the range of 5.3−5.5 eV at the CIS level, 6.2−6.3 eV region at the TD-B3LYP level, and at 5.48 eV at the MCQDPT2 level. The existence of such a transition has neither been observed in the vapor spectra nor in the aqueous solution. However, CD spectra of deoxyinosine 5′-phosphate show a weak peak near 225 nm (5.51 eV) which corresponds to a minimum in the absorption, and such a transition has been suggested because of the existence of a weak $\pi\pi^*$ or nπ^* transition.[23] The 5.48 eV transition obtained at the MCQDPT2 level in the gas phase is expected to be blue-shifted in the hydrogen-bonded environment because the dipole moment of this state is lower than the ground-state dipole moment at the CASSCF level. This transition is in excellent agreement with the CD prediction of the 5.51 eV region transition.[23] Therefore, it appears that our computed results resolve ambiguity of the nature of the 5.51 eV experimental transition in favor of the existence of a weak $\pi\pi^*$ transition. It is well-known that, for

TABLE 3: Ground and Lowest Singlet $\pi\pi^*$ and nπ^* Excited-State Geometrical Parameters of Hypoxanthine and Its Hydrated Form[a]

	S_0		1-$\pi\pi^*$				S_0		1-$\pi\pi^*$		
		+3W		+3W	1-nπ^*			+3W		+3W	1-nπ^*
C2N1	1.353	1.349	1.377	1.377	1.353	C5C4N9	105.5	105.8	104.3	104.5	105.3
N3C2	1.275	1.279	1.370	1.374	1.274	N7C8N9	112.9	113.1	114.0	114.2	112.6
C4N3	1.361	1.361	1.290	1.291	1.371	C4N9C8	106.3	106.2	106.3	106.4	106.4
C5C4	1.366	1.367	1.424	1.425	1.361	O6C6N1	120.2	120.4	121.4	122.0	116.5
C6N1	1.410	1.399	1.428	1.412	1.433	O6C6C5	130.6	129.4	128.3	127.1	116.4
C6C5	1.442	1.434	1.461	1.460	1.469	H1N1C2	119.0	119.1	116.9	117.6	117.5
N7C5	1.374	1.375	1.354	1.353	1.367	H2C2N3	119.4	119.4	119.5	119.4	119.0
C8N7	1.280	1.283	1.293	1.299	1.286	H8C8N9	121.6	121.6	121.5	121.7	121.9
N9C4	1.354	1.352	1.370	1.368	1.357	H9N9C8	127.6	128.6	127.2	128.7	127.5
N9C8	1.370	1.364	1.361	1.352	1.365	N3C2N1C6	0.0	0.2	−58.6	57.8	2.0
O6C6	1.189	1.201	1.182	1.191	1.278	C4N3C2N1	0.0	0.0	45.4	−44.9	−3.4
H1N1	0.997	1.003	0.997	1.002	0.994	C5C4N3C2	0.0	−0.1	−7.4	7.2	1.4
H2C2	1.076	1.075	1.072	1.071	1.077	C6C5C4N3	0.0	−0.1	−16.6	16.8	2.0
H8C8	1.071	1.071	1.072	1.071	1.071	N7C5C4N3	180.0	180.0	−177.2	177.6	176.8
H9N9	0.993	0.999	0.993	1.000	0.993	C5C6N1C2	0.0	−0.3	28.6	−27.7	1.6
N1C2N3	125.1	125.3	118.6	119.1	126.6	N1C6C5N7	180.0	−179.8	161.3	−161.9	175.3
C2N3C4	112.3	112.4	110.1	110.0	112.2	C8N7C5C4	0.0	0.0	−1.8	1.8	0.7
N3C4C5	128.4	127.7	125.0	124.7	128.5	N9C8N7C5	0.0	0.0	2.2	−2.1	−0.1
C2N1C6	126.0	125.4	114.3	114.3	124.4	O6C6C5C4	180.0	−179.8	−173.5	172.7	131.5
C4C5C6	119.0	119.0	118.6	118.7	118.7	N3C2N1H1	180.0	−179.9	167.0	−165.5	170.6
N1C6C5	109.3	110.2	110.3	110.9	109.5	H2C2N1C6	180.0	−179.9	138.3	−139.7	−177.4
C4C5N7	110.4	110.2	110.0	109.8	110.8	H8C8N7C5	180.0	180.0	−177.9	178.1	179.9
C5N7C8	104.8	104.7	105.3	105.2	104.8	H9N9C8N7	180.0	180.0	178.7	179.3	178.3

[a] The "+3W" represents the corresponding hydrated form.

purines such as adenine and guanine, the 260 (4.77) and 200 nm (6.20 eV) absorption bands are composite in nature.[21,34] Similar trends have also been found for hypoxanthine in which the MCD spectra suggest that the 260 and 200 nm absorption bands of hypoxanthine are composed of at least two transitions and that their transition moment directions are nonparallel to each other.[22] Two components of the 260 nm band are observed near 4.41 and 5.19 eV in the vapor phase and near 4.59−4.77 and 4.98 eV in aqueous solution in the case of 9-methylhypoxanthine.[33] For the 200 nm band in the vapor phase, the spectra of 9-methylhypoxanthine show transitions near 6.05 and 6.42 eV, while in an aqueous environment such resolution is not obtained.[33] The observed splitting of the 260 and 200 nm transitions is also revealed in our computations. The computed transition moment directions at the TD-B3LYP and CIS levels generally support the nonparallelism of the corresponding transition moment directions (Table 1).

Clark has suggested the existence of nπ^* transitions near 5.08 and 6.08 eV in 2-deoxyadenosine[34a] and near 5.21 and 6.32 eV for the model spectrum of guanine[34b] from the single-crystal polarized absorption and reflection measurements. To the best of our knowledge, the experimental information about nπ^* transitions of hypoxanthine is not available. However, because hypoxanthine is structurally more similar to guanine than adenine, the experimental knowledge regarding the nπ^* transitions of guanine can be used to predict the nπ^* transitions of hypoxanthine. MCQDPT2 calculations predict nπ^* transitions near 5.75 and 6.06 eV; however, these transition energies are expected to increase under hydrogen-bonding environments. The TD-B3LYP method predicts the nπ^* transitions for the hydrated hypoxanthine at 5.4 and 5.5 eV, while the CIS method predicts such transitions near 5.18 and 5.56 eV (Table 1). It appears from the above discussion that the first two nπ^* transitions of hypoxanthine may be located near the 5.2 and 6.1 eV region.

3.2. Excited-State Geometries. The ground-state geometry of hypoxanthine is planar in the isolated and hydrated forms. The geometries in the lowest singlet $\pi\pi^*$ excited state is appreciably nonplanar. Such out-of-plane deformation is localized mainly around the N1−C2 bond in the six-membered ring. The geometry of the molecule in this state is shown in Figure 1b. This figure clearly shows that the C2H part is appreciably out-of-plane compared to the rest of the ring. The geometrical parameters computed at the HF and CIS levels in the ground and excited states are shown in Table 3. This table suggests that in going from the ground state to the lowest singlet $\pi\pi^*$ excited state, the C2N1, N3C2, and C5C4 bond lengths are increased by about 0.024, 0.095, and 0.058 Å, respectively, while the C4N3 bond length is decreased by about 0.070 Å. A significant change in the geometrical parameters is not found in going from the isolated to the hydrated form. In going from the ground state to the lowest singlet nπ^* excited state, significant out-of-plane displacement in the C6O6 group is revealed; however, the ring geometry is approximately planar (Figure 1c). The CO bond length is also increased appreciably by about 0.089 Å in this state as compared to the corresponding ground-state value (Table 3). In the case of the hydrated species, the hydrogen bond distances shown in Figure 1d do not reveal significant changes in going from the ground to the lowest singlet $\pi\pi^*$ excited state. The geometrical deformation of hydrated hypoxanthine in the $\pi\pi^*$ excited state is similar to those predicted in the isolated form.

TABLE 4: Computed Minimum MEP Values ($-V_{min}$; kcal/mol) near the Different Sites of Hypoxanthine in the Ground and Vertical Singlet Excited States Obtained at the HF/6-311++G(d,p) and CIS/6-311++G(d,p) Levels

	$-V_{min}$		
states	N7	O6[a]	N3
S_0	70.3	70.3	45.8
1-$\pi\pi^*$	59.0	56.5	48.3
2-$\pi\pi^*$	64.6	63.4	32.6
1-nπ^*	70.3	23.2	57.7

[a] Values are located toward the N7 site at an angle of about 60° from the C6O6 direction, except for the 1-nπ^* excited state.

3.3. Molecular Electrostatic Potential and Electron Density Difference Maps. Ground and vertical singlet excited-state MEP maps obtained at the HF/6-311++G(d,p) and CIS/6-311++G(d,p) levels, respectively, are shown in Figure 2, while the minimum potential ($-V_{min}$) values at different sites are presented in Table 4. MEP features are modified in going

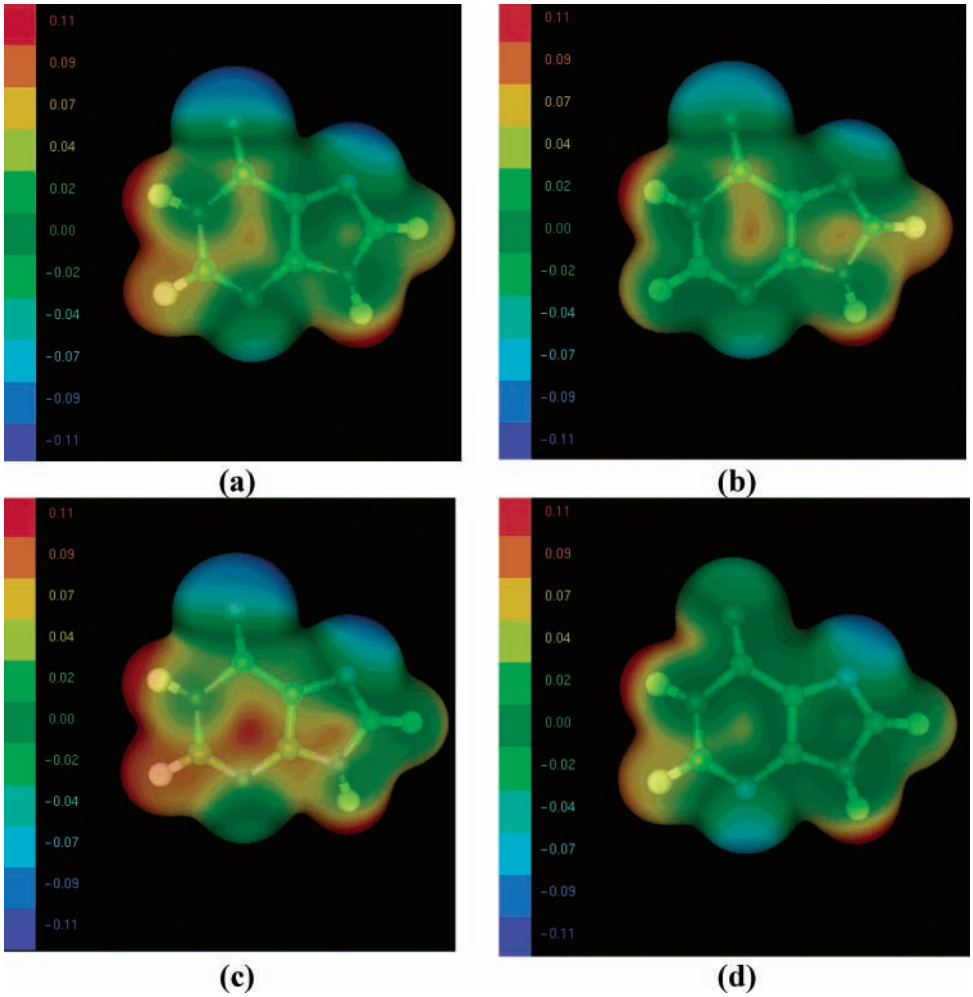

Figure 2. Hypoxanthine with molecular electrostatic potential mapped onto the electron density: (a) ground, (b) 1-$\pi\pi^*$, (c) 2-$\pi\pi^*$, and (d) 1-nπ^* state. The isosurface value is 0.005 with a range for the MEP of −0.11 to 0.11 au.

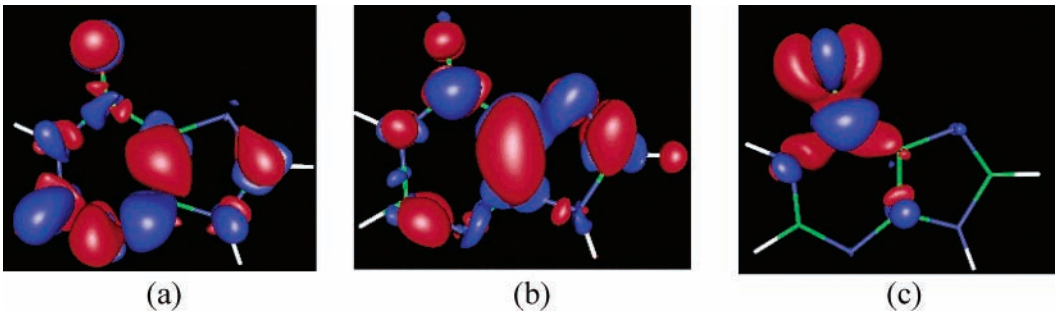

Figure 3. Density difference maps of hypoxanthine: (a) 1-$\pi\pi^*-S_0$, (b) 2-$\pi\pi^*-S_0$, and (c) 1-nπ^*-S_0. The blue and red show the increase and decrease in electron density, respectively. The isosurface for (a) and (b) corresponds to 0.003, while for (c) it corresponds to 0.007 au. The red indicates the negative and blue indicates the positive isosurface.

from the ground to different excited states (Figure 2). Data shown in Table 4 suggest that, in the ground state, the minimum potential values at the N7 and O6 sites are the same, while at the N3 site it is significantly weaker. In going from the ground state to the $\pi\pi^*$ singlet excited states, potential magnitudes at the N7 and O6 sites are reduced, while at the N3 site it is slightly increased for the first singlet $\pi\pi^*$ (1-$\pi\pi^*$) excited state but significantly reduced for the second singlet $\pi\pi^*$ (2-$\pi\pi^*$) excited state. A significant difference is also revealed between the MEP values of the two $\pi\pi^*$ states. The MEP magnitudes at the N7 and O6 sites are weaker in the 1-$\pi\pi^*$ state than the corresponding sites in the 2-$\pi\pi^*$ excited state; the reverse is true for the N3 site for these two states. In going from the ground state to the lowest singlet nπ^* (1-nπ^*) excited state, although the minimum potential value at the N7 site remains the same, at the N3 site it is increased. A most significant feature is observed in terms of the large reduction of potential magnitude at the O6 site of the molecule in this state (1-nπ^*). The large reduction in the minimum potential value at the O6 site can be explained in terms of the characterization of this state as being due to the excitation of the carbonyl lone pair electrons. Thus, the above discussion reveals that the MEP features are significantly changed in going from the ground state to the different vertical singlet excited states.

The electron density difference maps obtained by subtracting the ground-state electronic density from the excited-state density are presented in Figure 3. The density difference maps clearly show the migration of densities in going from the ground state

to different vertical singlet excited states of hypoxanthine. In going from the ground state to the first vertical singlet $\pi\pi^*$ excited state, density is modified mainly around the C2−N3−C4−C5, C8−N9, and carbonyl part of the molecule. In the case of the second vertical singlet $\pi\pi^*$ excited state, the density is modified mainly in the C4−C5−N7−C8 and C6O6 part of the molecule. In going from the ground state to the lowest singlet $n\pi^*$ excited state, the change in charge density is localized mainly at and around the carbonyl group of the molecule.

4. Conclusions

Computed transition energies of hypoxanthine obtained at the MCQDPT2 level are generally in agreement within an accuracy of 0.2 eV with the experimental transition energies. Our study resolves the existing ambiguity of the 225 nm transition in favor of a weak $\pi\pi^*$ transition. The excited-state geometry of the isolated and hydrated forms of the molecule in the lowest singlet $\pi\pi^*$ excited state is found to be highly distorted, and such out-of-plane deformation is localized in the six-membered ring of the molecule. The MEP features are significantly modified in going from the ground state to different vertical singlet excited states. The MEP maps are also quite different among the vertical singlet $\pi\pi^*$ excited states. As compared to the ground state, the potential magnitude in the vertical singlet $n\pi^*$ excited state is drastically reduced at the carbonyl oxygen site which is involved in the $n\pi^*$ excitation.

Acknowledgment. We are thankful for NIH-RCMI Grant No. G1 2RR13459-21, NSF-CREST Grant No. 9805465 and 9706268, ONR Grant No. N00034-03-1-0116, and NSF-EPSCoR Grant No. 300423-190200-21000 for financial assistance. We also thank Prof. A. Sadlej, Department of Chemistry, Nicolaus Copernicus University at Torun, Poland, for useful discussions.

References and Notes

(1) (a) Lewis, G. N.; Kasha, M. *J. Am. Chem. Soc.* **1944**, *66*, 2100. (b) Kasha, M.; Sytnik, A.; Dellinger, B. *Pure Appl. Chem.* **1993**, *65*, 1641. (c) Sytnik, A.; Kasha, M. *Proc. Natl. Acad. Sci. U.S.A.* **1994**, *91*, 8627. (d) Sytnik, D.; Gormin, D.; Kasha, M. *Proc. Natl. Acad. Sci. U.S.A.* **1994**, *91*, 11968. (e) Gormin, D.; Heldt, J.; Kasha, M. *J. Phys. Chem.* **1995**, *99*, 7281. (f) Kasha, M. *Acta Phys. Pol., A* **1999**, *95*, 15.

(2) Kasha, M. *Faraday Discuss. Chem. Soc.* **1950**, *9*, 14.

(3) Taylor, C. A.; El-Bayoumi, A. M.; Kasha, M. *Proc. Natl. Acad. Sci. U.S.A.* **1969**, *65*, 253.

(4) (a) Shukla, M. K.; Leszczynski, J. *J. Phys. Chem. A* **2002**, *106*, 1011. (b) Shukla, M. K.; Leszczynski, J. *J. Phys. Chem. A* **2002**, *106*, 8642. (c) Shukla, M. K.; Leszczynski, J. *J. Phys. Chem. A* **2002**, *106*, 4709. (d) Shukla, M. K.; Leszczynski, J. *J. Phys. Chem. A* **2002**, *106*, 11338.

(5) (a) Brady, B. B.; Peteanu, L. A.; Levy, D. H. *Chem. Phys. Lett.* **1988**, *147*, 538. (b) Chinsky, L.; Laigle, A.; Peticolas, L.; Turpin, P.-Y. *J. Chem. Phys.* **1982**, *76*, 1.

(6) Shukla, M. K.; Mishra, P. C. *Chem. Phys.* **1999**, *240*, 319.

(7) (a) Kerr, R. A. *Science* **1998**, *280*, 202. (b) Baird, C. *Environmental Chemistry*; W. H. Freeman: New York, 1995.

(8) (a) Darnell, J.; Lodish, H.; Baltimore, D. *Molecular Cell Biology*; Scientific American Books: New York, 1986; p 553. (b) Taylor, J.-S. *Chem. Educ.* **1990**, *67*, 835.

(9) (a) Lowdin, P. O. *Rev. Mod. Phys.* **1963**, *35*, 724. (b) Lowdin, P. O. In *Electronic Aspects of Biochemistry*; Pullman, B., Ed.; Academic Press: New York, 1964; p 167. (c) Lowdin, P. O. *Mutat. Res.* **1965**, *2*, 218. (d) Lowdin, P. O. *Adv. Quantum Chem.* **1965**, *2*, 213.

(10) Stryer, L. *Biochemistry*, 3rd ed.; Freeman: New York, 1988.

(11) Friedberg, E. C.; Walker, G. C.; Siede, W. *DNA Repair and Mutagenesis*; ASM Press: Washington, DC, 1995.

(12) (a) Holley, R. W.; Apgar, J.; Everett, G. A.; Madison, J. T.; Marquisee, M.; Merrill, S. H.; Penswick, J. R.; Zamir, A. *Science* **1965**, *147*, 1462. (b) Dutting, D.; Karau, W.; Melchers, F.; Zachau, H. G. *Biochim. Biophys. Acta* **1965**, *108*, 194. (c) Grunberger, D.; Holy, A.; Sorm, F. *Biochim. Biophys. Acta* **1967**, *134*, 484.

(13) (a) Ramaekers, R.; Maes, G.; Adamowicz, L.; Dkhissi, A. *J. Mol. Struct.* **2001**, *560*, 205. (b) Sheina, G. G.; Stepanian, S. G.; Radchenko, E. D.; Blagoi, Yu. P. *J. Mol. Struct.* **1987**, *158*, 275.

(14) (a) Shukla, M. K.; Leszczynski, J. *J. Phys. Chem. A* **2000**, *104*, 3021. (b) Shukla, M. K.; Leszczynski, J. *J. Mol. Struct. (THEOCHEM)* **2000**, *529*, 99. (c) Hernandez, B.; Luque, F. T.; Orozco, M. *J. Org. Chem.* **1996**, *61*, 5964. (d) Costas, M. E.; Acevedo-Chavez, R. *J. Phys. Chem. A* **1997**, *101*, 8309.

(15) Lin, J.; Yu, C.; Peng, S.; Akiyama, I.; Li, K.; Lee, L. K.; LeBreton, P. R. *J. Phys. Chem.* **1980**, *84*, 1006.

(16) Chenon, M. T.; Pugmire, R. J.; Grant, D. M.; Panzica, R. P.; Townsend, L. B. *J. Am. Chem. Soc.* **1975**, *97*, 4636.

(17) Lichtenberg, D.; Bergmann, F.; Neiman, Z. *Isr. J. Chem.* **1972**, *10*, 805.

(18) Munns, A. R. I.; Tollin, P. *Acta Crystallogr., Sect. B* **1970**, *26*, 1101.

(19) Sadeghi, R. R.; Cheng, H.-P. *J. Chem. Phys.* **1999**, *111*, 2086.

(20) Douhal, A.; Kim, S. K.; Zewail, A. H. *Nature (London)* **1995**, *378*, 260.

(21) Callis, P. R. *Annu. Rev. Phys. Chem.* **1983** *34*, 329.

(22) (a) Sutherland, J. C.; Griffin, K. *Biopolymers* **1984**, *23*, 2715. (b) Voelter, W.; Records, R.; Bunnenberg, E.; Djerassi, C. *J. Am. Chem. Soc.* **1968**, *90*, 6163.

(23) Sprecher, C. A.; Johnson, W. C., Jr. *Biopolymers* **1977**, *16*, 2243.

(24) Nakano, H. *J. Chem. Phys.* **1993**, *99*, 7983.

(25) Foresman, J. B.; Head-Gordon, M.; Pople, J. A.; Frisch, M. J. *J. Phys. Chem.* **1992**, *96*, 135.

(26) (a) Casida, M. E.; Jamorski, C.; Casida, K. C.; Salahub, D. R. *J. Chem. Phys.* **1998**, *108*, 4439. (b) Robb, M. A.; Garavelli, M.; Olivucci, M.; Bernardi, F. In *Reviews in Computational Chemistry*; Lipkowitz, K. B., Boyd, D. B., Eds.; Wiley-VCH: New York, 2000; Vol. 15, p 87.

(27) (a) Laaksonen, L. *J. Mol. Graphics* **1992**, *10*, 33. (b) Bergman, D. L.; Laaksonen, L.; Laaksonen, A. *J. Mol. Graphics Modell.* **1997**, *15*, 301.

(28) (a) Frisch, M. J.; Trucks, G. W.; Schlegel, H. B.; Gill, P. M. W.; Johnson, B. G.; Robb, M. A.; Cheeseman, J. R.; Keith, T.; Petersson, G. A.; Montgomery, J. A.; Raghavachari, K.; Al-Laham, M. A.; Zakrzewski, V. G.; Ortiz, J. V.; Foresman, J. B.; Cioslowski, J.; Stefanov, B. B.; Nanayakkara, A.; Challacombe, M.; Peng, C. Y.; Ayala, P. Y.; Chen, W.; Wong, M. W.; Andres, J. L.; Replogle, E. S.; Gomperts, R.; Martin, R. L.; Fox, D. J.; Binkley, J. S.; Defrees, D. J.; Baker, J.; Stewart, J. P.; Head-Gordon, M.; Gonzalez, C.; Pople, J. A. *Gaussian 94*, revision E.2; Gaussian, Inc.: Pittsburgh, PA, 1995. (b) Frisch, M. J.; Trucks, G. W.; Schlegel, H. B.; Scuseria, G. E.; Robb, M. A.; Cheeseman, J. R.; Zakrzewski, V. G.; Montgomery, J. A., Jr.; Stratmann, R. E.; Burant, J. C.; Dapprich, S.; Millam, J. M.; Daniels, A. D.; Kudin, K. N.; Strain, M. C.; Farkas, O.; Tomasi, J.; Barone, V.; Cossi, M.; Cammi, R.; Mennucci, B.; Pomelli, C.; Adamo, C.; Clifford, S.; Ochterski, J.; Petersson, G. A.; Ayala, P. Y.; Cui, Q.; Morokuma, K.; Malick, D. K.; Rabuck, A. D.; Raghavachari, K.; Foresman, J. B.; Cioslowski, J.; Ortiz, J. V.; Baboul, A. G.; Stefanov, B. B.; Liu, G.; Liashenko, A.; Piskorz, P.; Komaromi, I.; Gomperts, R.; Martin, R. L.; Fox, D. J.; Keith, T.; Al-Laham, M. A.; Peng, C. Y.; Nanayakkara, A.; Challacombe, M.; Gill, P. M. W.; Johnson, B.; Chen, W.; Wong, M. W.; Andres, J. L.; Gonzalez, C.; Head-Gordon, M.; Replogle, E. S.; Pople, J. A. *Gaussian 98*, revision A.9; Gaussian, Inc.: Pittsburgh, PA, 1998.

(29) Schmidt, M. W.; Baldridge, K. K.; Boatz, J. A.; Elbert, S. T.; Gordon, M. S.; Jensen, J. H.; Koseki, S.; Matsunga, N.; Nguyen, K. A.; Su, S. J.; Windus, T. L.; Dupuis, M.; Montgomery, J. A. *J. Comput. Chem.* **1993**, *14*, 1347.

(30) Broo, A.; Holmen, A. *J. Phys. Chem. A* **1997**, *101*, 3589.

(31) Aaron, J.-J.; Gaye, M. D.; Parkanyi, C.; Cho, N. S.; Szentpaly, L. V. *J. Mol. Struct.* **1987**, *156*, 119.

(32) (a) Sobolewski, A. L.; Domcke, W. *Chem. Phys. Lett.* **1999**, *300*, 533. (b) Sobolewski, A. L.; Domcke, W. *Chem. Phys.* **2000**, *259*, 181. (c) Sobolewski, A. L.; Domcke, W. *Chem. Phys. Lett.* **1999**, *315*, 293.

(33) (a) Clark, L. B.; Tinoco, I., Jr. *J. Am. Chem. Soc.* **1965**, *87*, 11. (b) Clark, L. B.; Peschel, G. G.; Tinoco, I., Jr. *J. Phys. Chem.* **1965**, *69*, 3615.

(34) (a) Clark, L. B. *J. Phys. Chem.* **1995**, *99*, 4466. (b) Clark, L. B. *J. Am. Chem. Soc.* **1994**, *116*, 5265. (c) Clark, L. B. *J. Phys. Chem.* **1990**, *94*, 2873.